Supporting Information

Spontaneous and Rapid Electrostatic Solvent Nanofiltration based on Conductive Layered Membrane

Song Song, [‡ a,b] Haozhe Sun, [‡ b,c] Jiaxiang Xia,[a,b] Shiwen Bao,[a,b] Wenbin Ding,[a] Nuo Liu,[a] Tianwen Wang,[a] Kunyan Sui, *[a] Jun Gao, *[b,d,e] Xueli Liu*[a] and Lei Jiang[f]

[a] State Key Laboratory of Bio-Fibers and Eco-textiles, College of Materials Science and Engineering, Shandong Collaborative Innovation Center of Marine Biobased Fibers and Ecological Textiles, Qingdao University, Qingdao 266071, P. R. China
[b] Qingdao Institute of Bioenergy and Bioprocess Technology, Chinese Academy of Sciences, Qingdao 266101, P. R. China
[c] State Key Laboratory of Heavy Oil Processing, College of Chemistry and Chemical Engineering, China University of Petroleum (East China), Qingdao 266580, P. R. China
[d] Shandong Energy Institute, Qingdao 266101, P. R. China
[e] Qingdao New Energy Shandong Laboratory, Qingdao 266101, P. R. China
[f] CAS Key Laboratory of Bio-inspired Materials and Interfacial Science, Technical Institute of Physics and Chemistry Chinese Academy of Sciences, Beijing 100190, P. R. China
*Corresponding authors: liuxl@qdu.edu.cn (X. Liu); jun.gao@qibebt.ac.cn (J. Gao); sky@qdu.edu.cn (K. Sui).

Table of Contents

Fig. S1 Optical image showing the Tyndall effect of the MXene suspension.

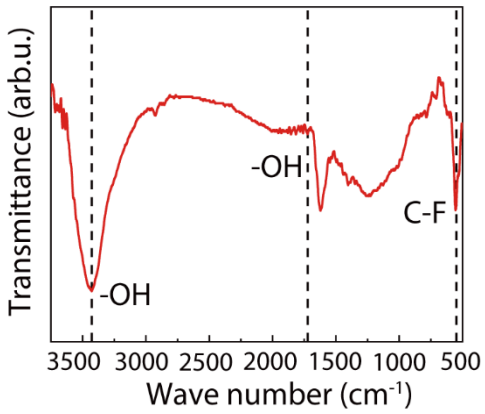

Fig. S2 FT-IR spectrum of the MXene nanosheets, exhibiting the characteristic peaks of MXene, namely the -OH and C-F peaks.

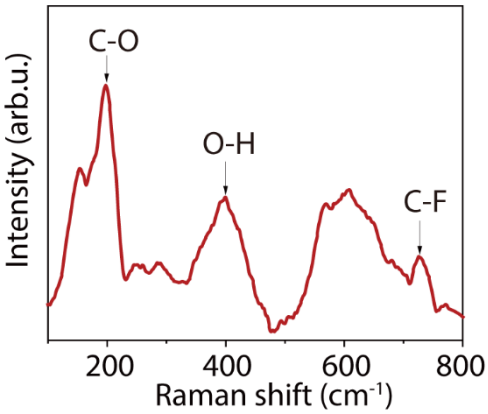

Fig. S3 Raman spectrum of the MXene membrane, showing the characteristic peaks of C-O, O-H, and C-F.

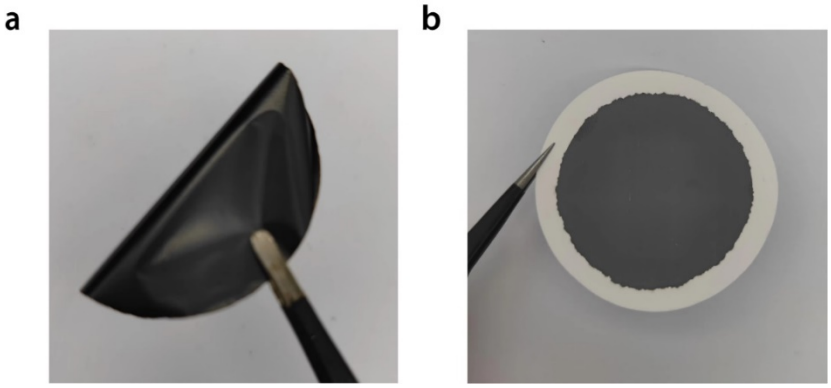

Fig. S4 Optical images of a free-standing MXene membrane (a) or one on a PVDF support (b).

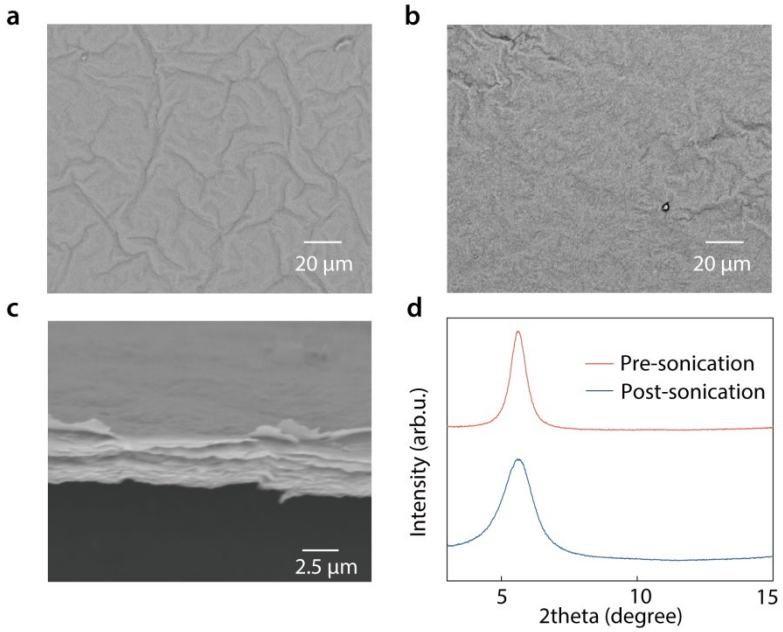

Fig. S5 Stability test of the MXene membrane by sonication treatment. (a, b) Surface SEM images of the membrane before (a) and after (b) sonication. (c) Cross-sectional SEM images of the membrane after sonication. (d) XRD patterns of the membrane before (red curve) after sonication (blue curve) in the wet state.

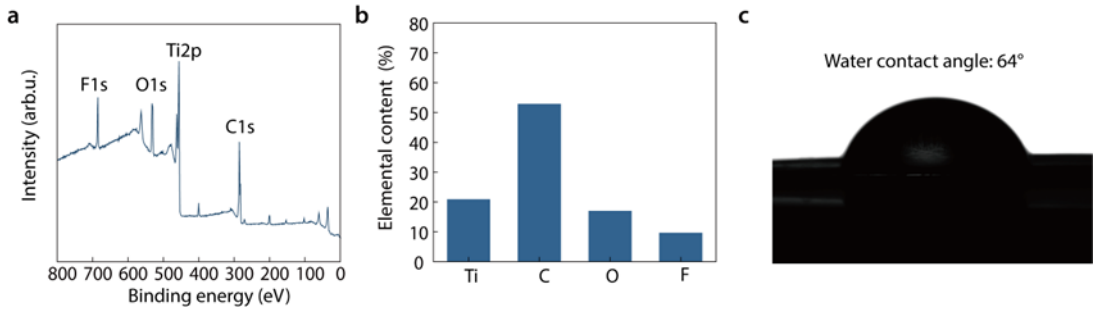

Fig. S6 The chemical and wettability analysis of the MXene membrane. (a) The XPS spectrum of MXene membranes and (b) the corresponding analysis of element content. (c) The contact angle of water on the MXene membrane.

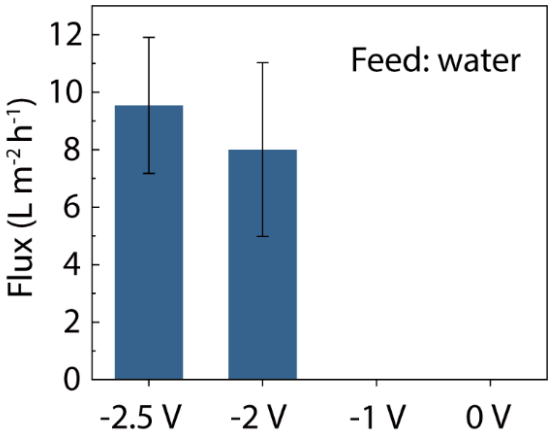

Fig. S7 The flux of water permeated through the MXene membrane as a function of the applied bias.

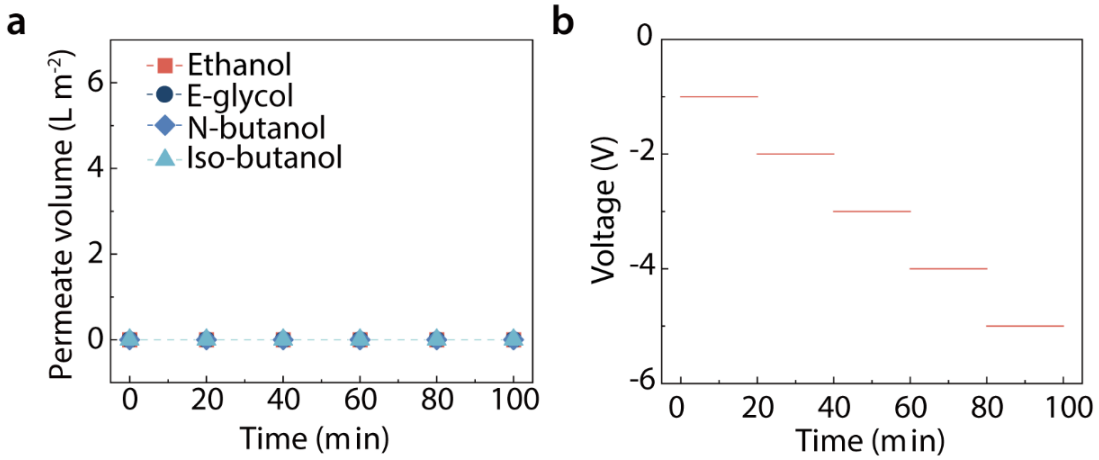

Fig. S8 Absence of electrical response for the permeation of single-component organic solvent. (a) The specific permeate volume for each solvent as a function of permeate time. (b) Step-wisely applied bias during the tests in (a).

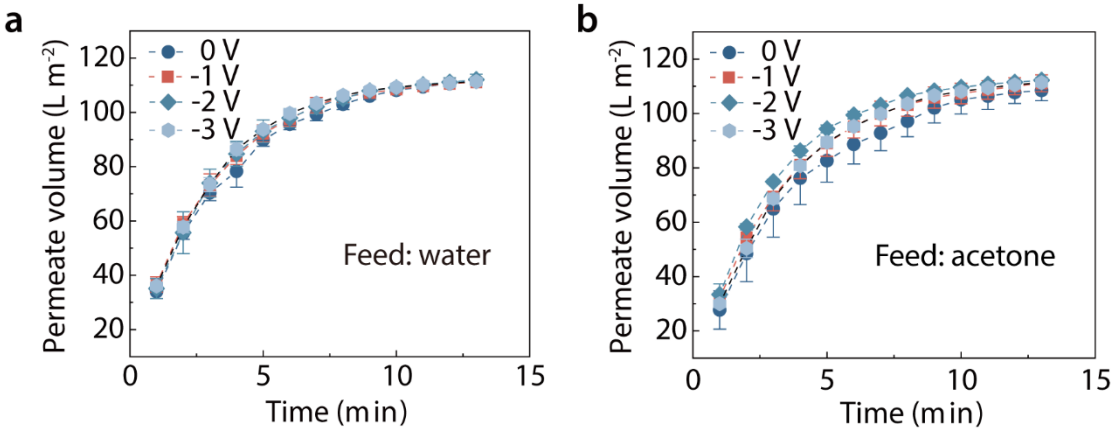

Fig. S9 Absence of electrical response for the permeation of water (a) and acetone (b) through the PVDF support substrate.

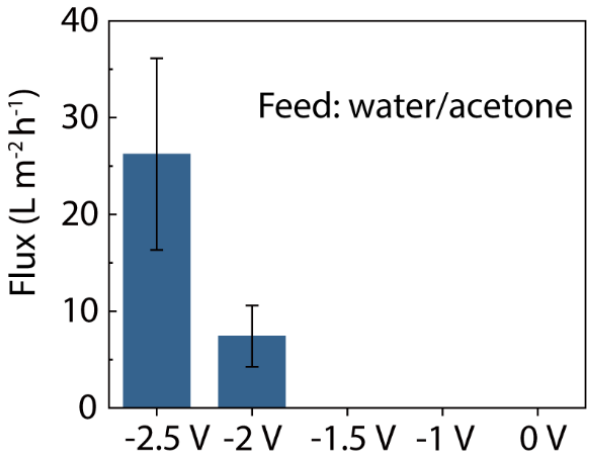

Fig. S10 The flux of permeate as a function of the applied bias when 120 nm thick MXene membrane was used. The volume ratio of acetone in the feed mixture was 10%.

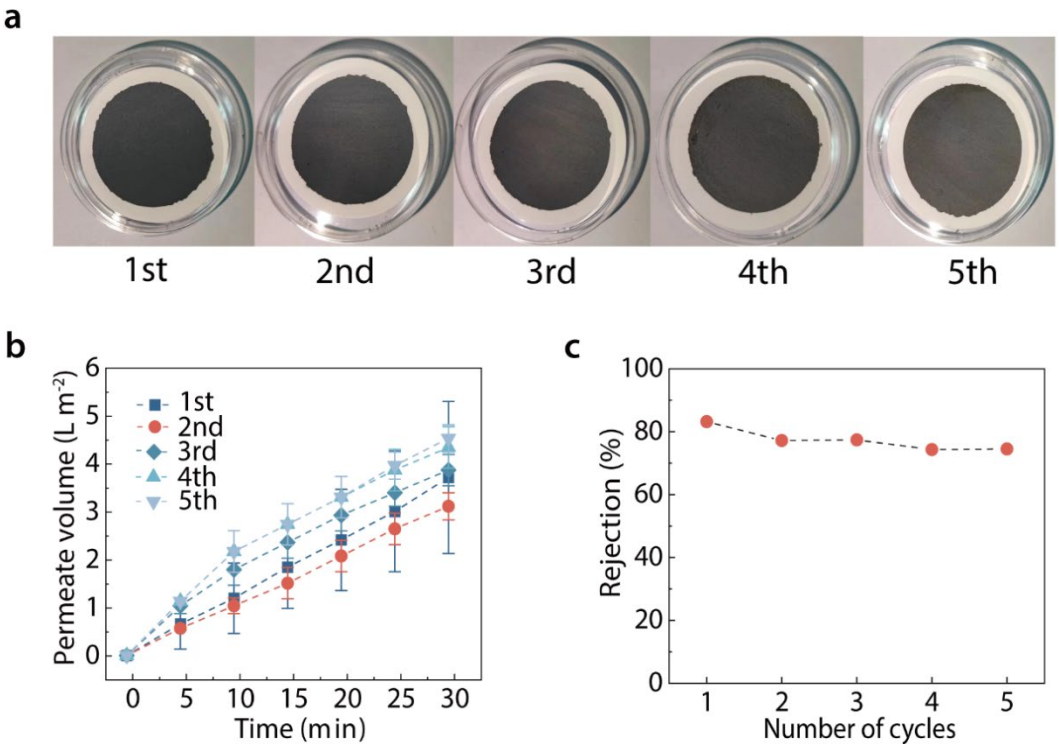

Fig. S11 Durability of the MXene membrane for ESN. (a) Optical images of the same MXene membrane after each separation process. Five cycles of separation were carried out for the durability investigation. (b) Specific permeate volume as a function of time during each cycle of separation. (c) The corresponding rejection rate of acetone for each separation. Water/acetone with 10 vol% of acetone was used for each separation process.

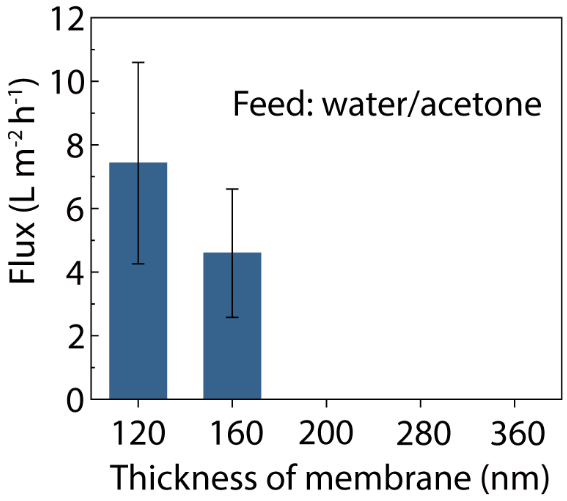

Fig. S12 The flux of permeate as a function of the membrane thickness, when the applied bias was -2 V. The volume ratio of acetone in the feed mixture was 10%.

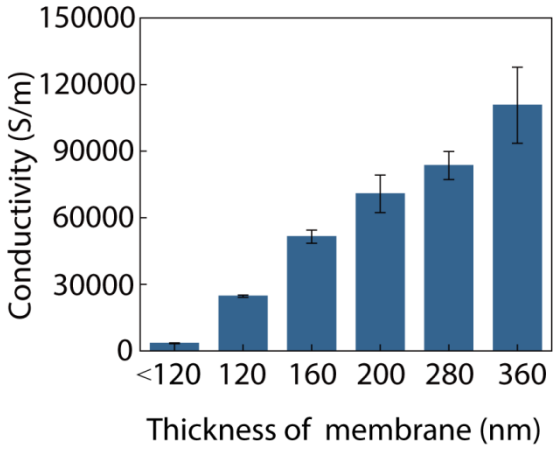

Fig. S13 The conductivity of MXene membranes with variable thickness.

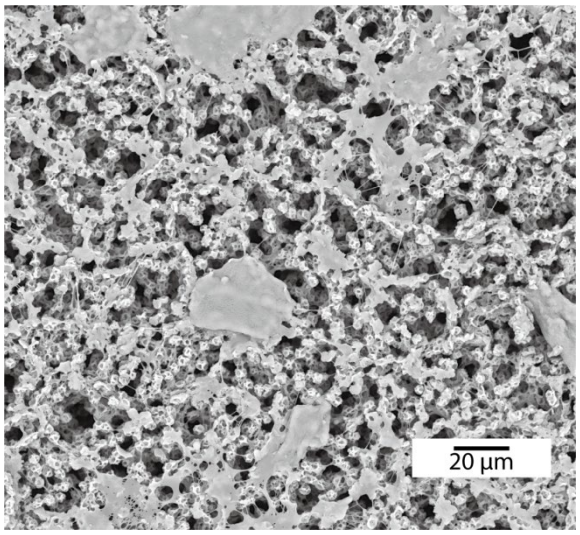

Fig. S14 SEM characterization of the MXene membrane with insufficient amount of MXene nanosheets used for membrane preparation (less than that used for membrane of 120 nm thick).

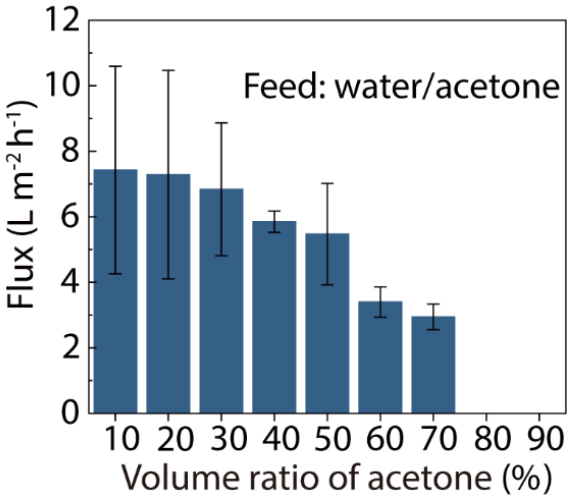

Fig. S15 The flux of permeate as a function of the volume ratio of acetone in the feed mixture. The applied bias was -2 V and the membrane thickness was 120 nm.

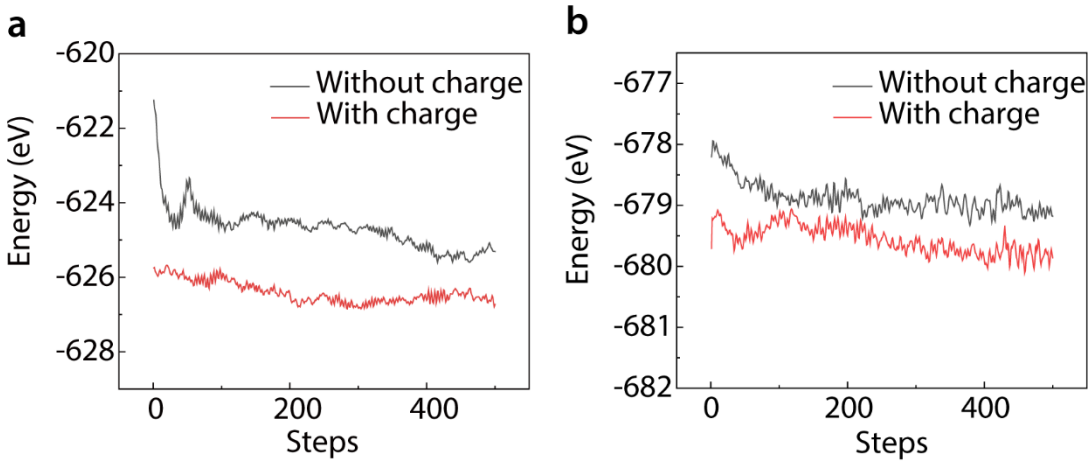

Fig. S16 Structural relaxation of the constructed unit cell under charged and uncharged conditions. (a) Structural relaxation of MXene cells with water; (b) with acetone.

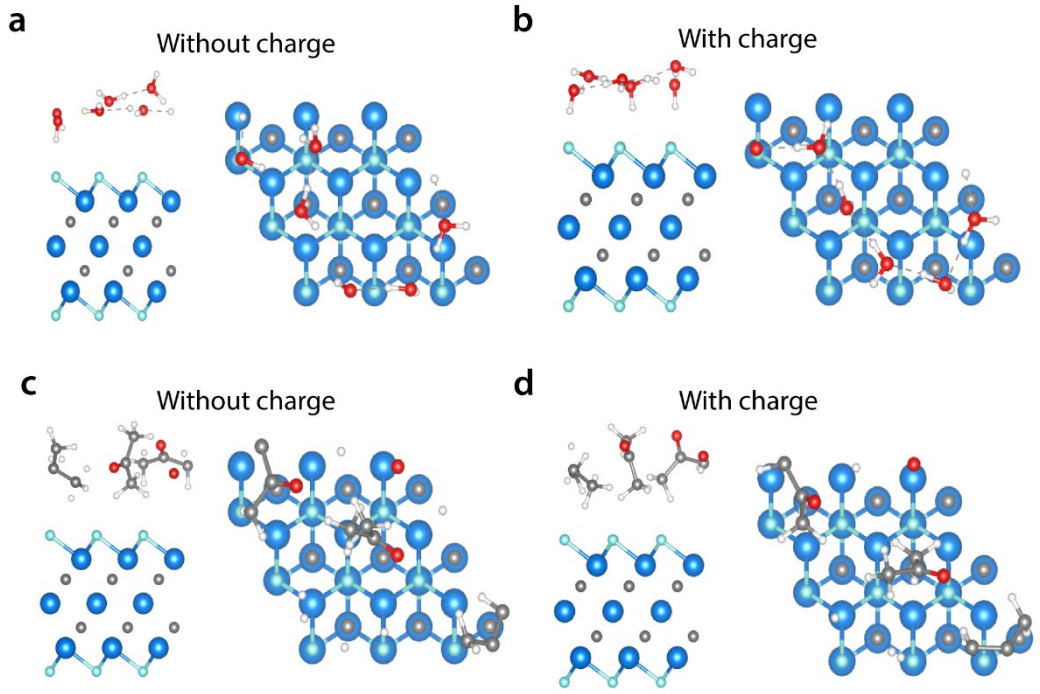

Fig. S17 DFT calculation of the water/MXene interaction (a, b) and acetone/MXene interaction (c, d) without (a, c) and with charge (b, d) added. Interaction sites with the lowest binding energy were used for the calculations. The left sides of (a-d) are the side views of the interaction, while the right sides are the top views which show the binding sites.

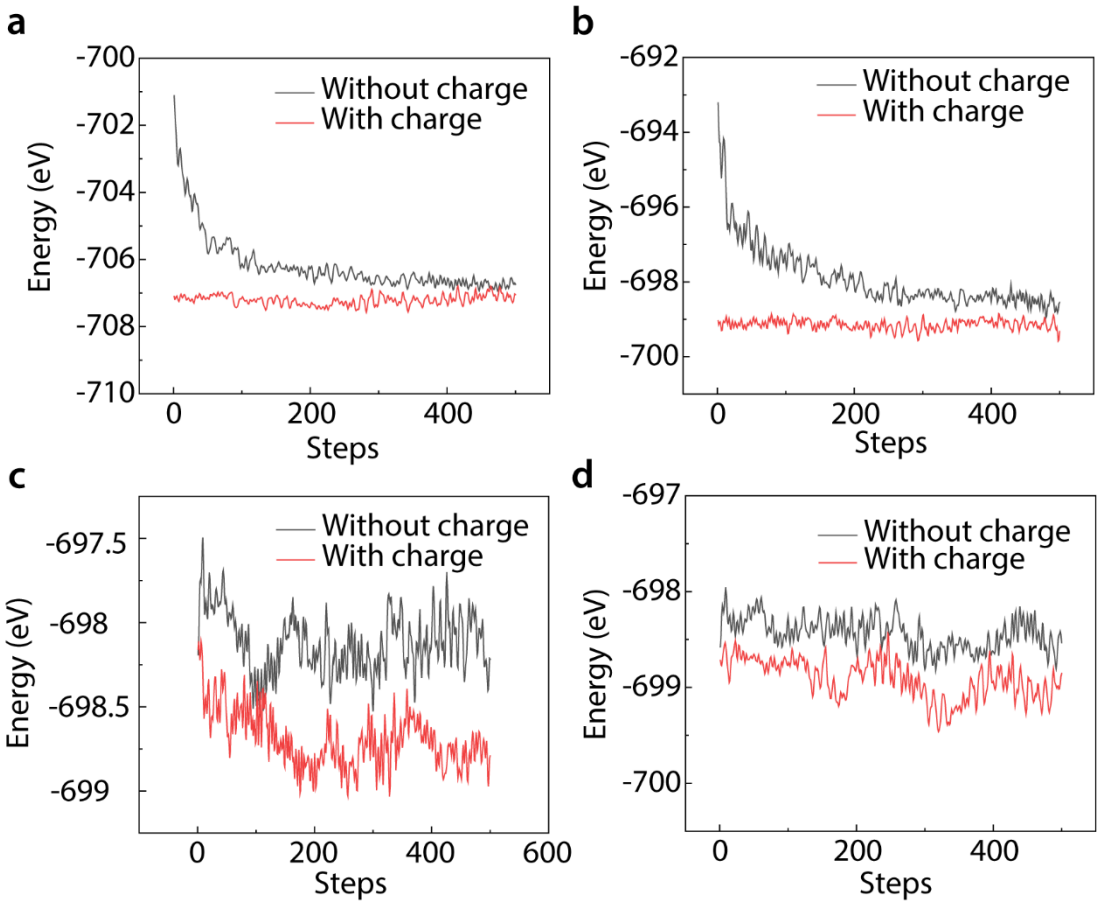

Fig. S18 Structural relaxation of the constructed unit cell under charged and uncharged conditions: (a) with ethanol; (b) with ethylene glycol; (c) with n-butanol; and (d) with iso-butanol.

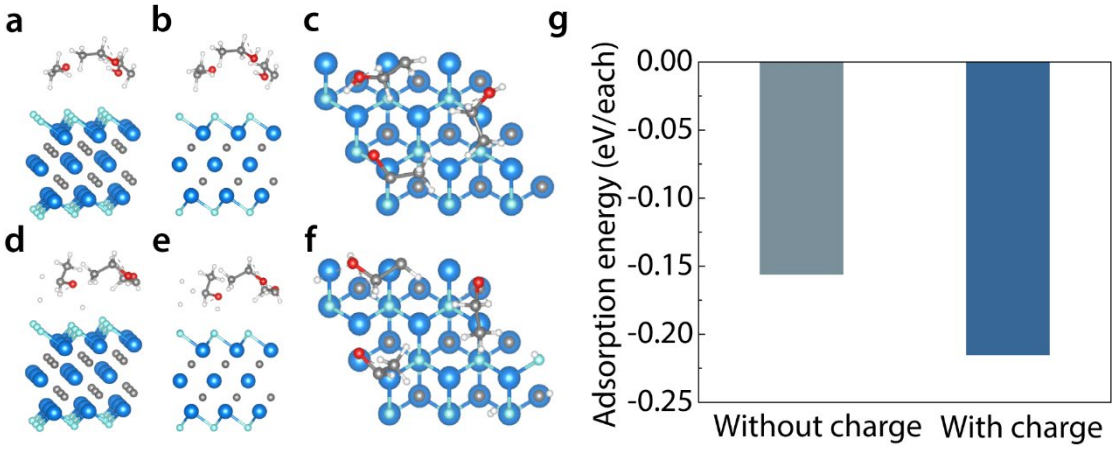

Fig. S19 DFT calculation of the ethanol/MXene interaction. (a, d) 3D views exhibiting the ethanol/MXene interaction without charge (a) and with charge (d). (b, e) Side views and (c, f) top views of the interaction without (b, c) and with (e, f) charge added. (g) The corresponding adsorption energy of ethanol on MXene surface without and with charge added. The results show that adding a negative charge enhances the ethanol/MXene interaction.

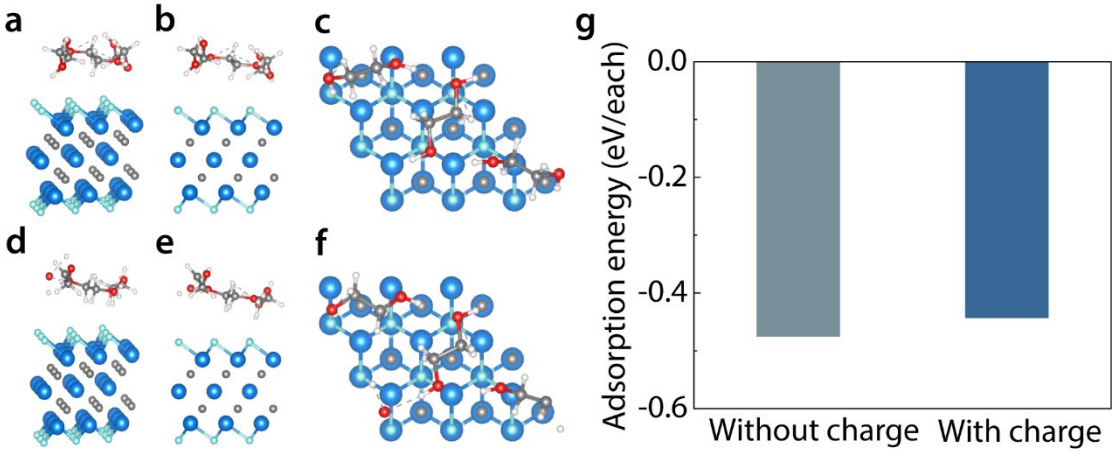

Fig. S20 DFT calculation of the ethylene glycol/MXene interaction. (a, d) 3D views exhibiting the ethylene glycol /MXene interaction without charge (a) and with charge (d). (b, e) Side views and (c, f) top views of the interaction without (b, c) and with (e, f) charge added. (g) The corresponding adsorption energy of ethylene glycol on MXene surface without and with charge added. The results show that adding a negative charge has almost no effect on the ethylene glycol/MXene interaction.

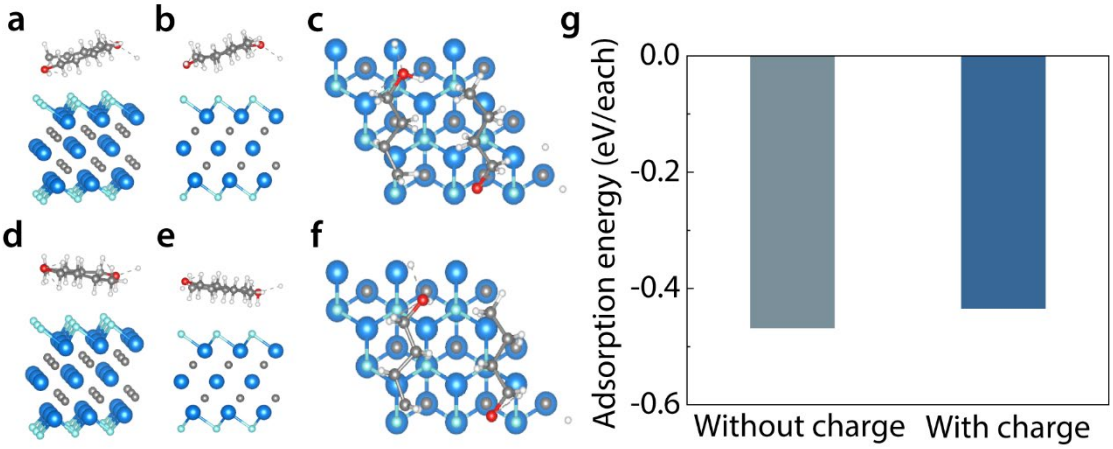

Fig. S21 DFT calculation of the n-butanol/MXene interaction. (a, d) 3D views exhibiting the n-butanol/MXene interaction without charge(a) and with charge (d). (b, e) Side views and (c, f) top views of the interaction without (b, c) and with (e, f) charge added. (g) The corresponding adsorption energy of n-butanol on MXene surface without and with charge added. The results show that adding a negative charge has almost no effect on the n-butanol/MXene interaction.

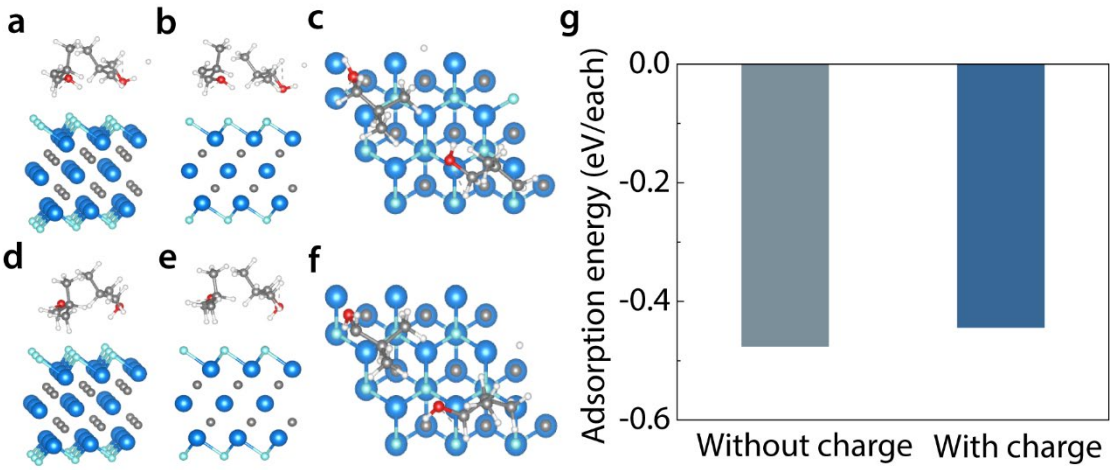

Fig. S22 DFT calculation of the iso-butanol/MXene interaction (a, d) 3D views exhibiting the iso-butanol/MXene interaction without charge (a) and with charge (d). (b, e) Side views and (c, f) top views of the interaction without (b, c) and with (e, f) charge added. (g) The corresponding adsorption energy of iso-butanol on MXene surface without and with charge added. The results show that adding a negative charge has almost no effect on the iso-butanol/MXene interaction.

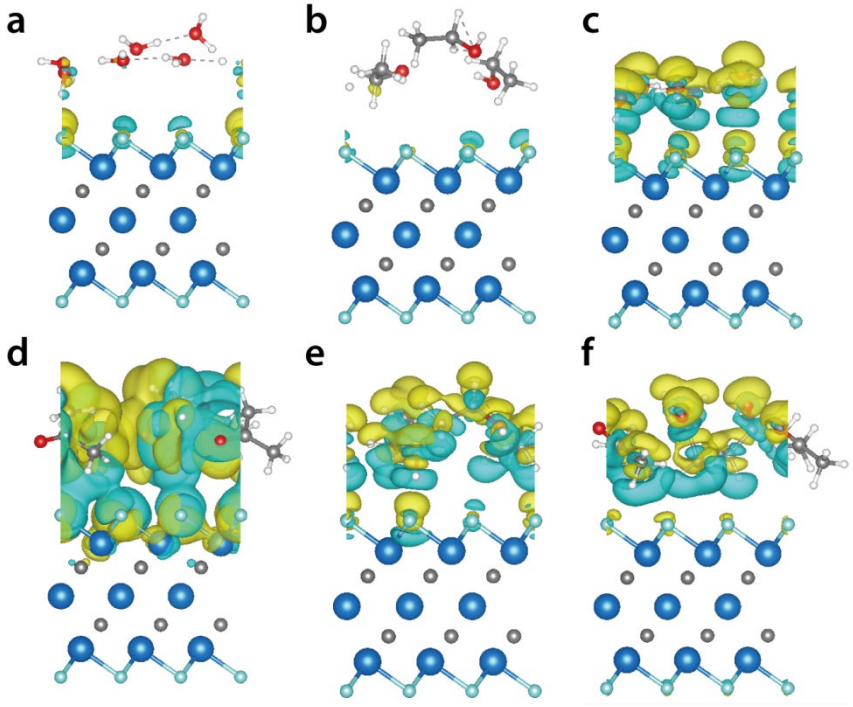

Fig. S23 DFT calculations of the differential charge density of water, acetone and ethanol on MXene surface before and after applying electric field. An isosurface value of 0.0005e/Bohr³ was used to illustrate the structural models and the differential charge density. Blue and yellow regions represent electron loss and gain, respectively. (a-c) The differential charge densities of water/MXene (a), ethanol/MXene (b) and acetone/MXene (c) before electric field application, and (d-f) after electric field application.

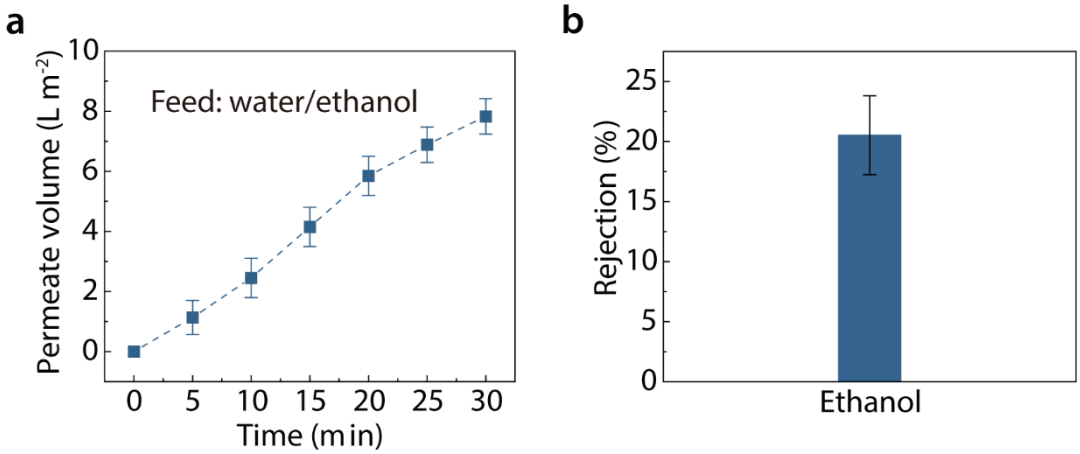

Fig. S24 Separation performance for the water/ethanol mixture. (a) The permeate volume as a function of permeate time. (b) The rejection rate of ethanol in the permeate. The volume ratio of ethanol in the feed mixture was 10 vol%.

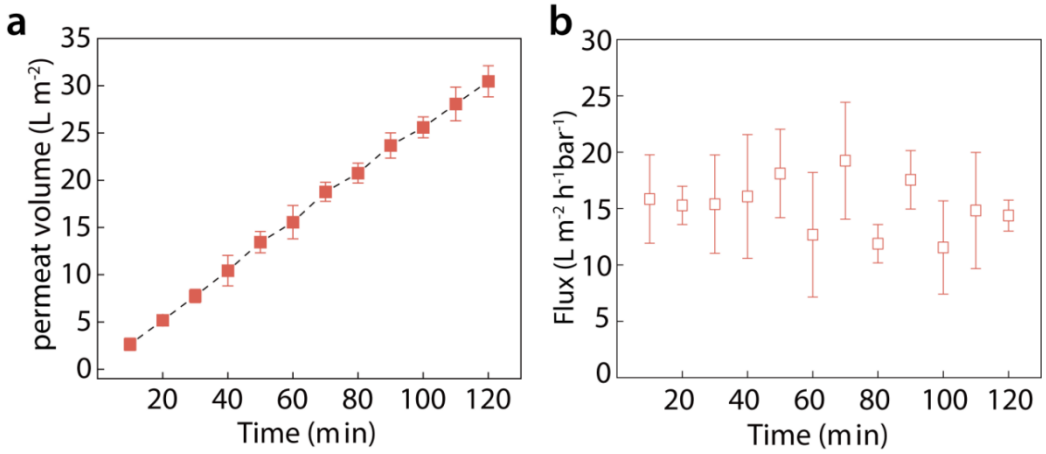

Fig. S25 Time-dependent permeate volume and permeate flux of water under an external pressure of 1 bar.

Table S1 Adsorption energy of water on MXene.

Added charge	E_{con}/eV	E_{MXene}/eV	E_{water}/eV	E_{ads}/eV
0	-626.17200228	-538.16516179	-87.56488714	-0.07365889
-1	-627.52904798	-538.86363618	-87.56488714	-0.18342077

Table S2 Adsorption energy of acetone on MXene.

Added charge	E_{con}/eV	E_{MXene}/eV	$E_{acetone}$ /eV	E_{ads}/eV
0	-707.71930261	-538.16516179	-168.94162956	-0.20417042
-1	-708.38504400	-538.86363618	-168.94162956	-0.19325942

Table S3 Adsorption energy of ethanol on MXene.

Added charge	E_{con}/eV	E_{MXene}/eV	$E_{ethanol}$/eV	E_{ads}/eV
0	-680.08294336	-538.16516179	-141.45043359	-0.15578266
-1	-680.95869441	-538.86363618	-141.45043359	-0.21487488

Table S4 Adsorption energy of ethylene glycol on MXene.

Added charge	E_{con}/eV	E_{MXene}/eV	$E_{ethylene\ glycol}$/eV	E_{ads}/eV
0	-700.03548526	-538.16516179	-161.00510124	-0.28840741
-1	-700.70749843	-538.86363618	-161.00510124	-0.27958700

Table S5 Adsorption energy of n-butanol on MXene.

Added charge	E_{con}/eV	E_{MXene}/eV	$E_{n\text{-}butanol}$/eV	E_{ads}/eV
0	-699.65636670	-538.16516179	-160.55459539	-0.46830476
-1	-700.28782025	-538.86363618	-160.55459539	-0.43479437

Table S6 Adsorption energy of iso-butanol on MXene.

Added charge	E_{con}/eV	E_{MXene}/eV	$E_{iso\text{-}butanol}$/eV	E_{ads}/eV
0	-699.39379238	-538.16516179	-160.27823148	-0.47519956
-1	-700.02865392	-538.86363618	-160.27823148	-0.44339313

Table S7 Comparison with previous works.

Materials	Method	Feed temperature (°C)	Feed	Flux (kg m^{-2} h^{-1})	Separation factor	Ref
ZIF-8 GO	PV	75	n-Butanol	0.606	23.7	1
ZIF-71/PEBA	PV	37	Acetone	0.025	8.2	2
			n-Butanol	0.0968	18.8	
ZIF8/PDMS	PV	80	n-Butanol	2.8005	52.81	3
COF-LZU1	PV	64	n-Butanol	2.694	38.7	4
CTF	PV	60	n-Butanol	2.816	62.8 ± 1.5	5
COF-LZU	PV	34	n-Butanol	0.629	20.4	6
IL-GO-PEBA	PV	60	n-Butanol	1.8283	32.5	7
P84/EDA	PV	50-60	Acetone	1.8	53	8
(PPMS)-CA	PV	40	Acetone	2.799	49.6	9
SHS/PDMS	PV	35	Acetone	0.535	46	10
PDMS/MOF-NS/PVDF	PV	40	Ethanol	6.8	8.9	11
			n-Butanol	9.4	12.1	
SPB/GO	PV	70	n-Butanol	5.23	8000	12
ACGMs	PV	20	Ethanol	35.6	18.4	13
		60		389.1	0.3	
PVDF-SWCNH	Membrane Distillation	57	Ethanol	12.3	-	14
BTESA	OSRO	50	Methanol/Toluene	0.09-1.6	4.9-32	15
MXene-PVDF	ESS	25	Acetone	7.4	4.05	This work
			n-Butanol	11.32	7.34	
			iso-Butanol	11.74	17.25	

OSRO: organic solvent reverse osmosis

The separation factor in the ESN system is calculated by the following equation:

$$\alpha = \frac{\left(\frac{Y_{water}}{1 - Y_{water}}\right)}{\left(\frac{X_{water}}{1 - X_{water}}\right)} \quad (1)$$

where X_{water} and Y_{water} denote the mass fraction of water in the feed and permeate, respectively.

References

1. W. Li, J. Li, N. Wang, X. Li, Y. Zhang, Q. Ye, S. Ji and Q.-F. An, Recovery of bio-butanol from aqueous solution with ZIF-8 modified graphene oxide composite membrane, *Journal of Membrane Science*, 2020, **598**, 117671.
2. S. Liu, G. Liu, X. Zhao and W. Jin, Hydrophobic-ZIF-71 filled PEBA mixed matrix membranes for recovery of biobutanol via pervaporation, *Journal of Membrane Science*, 2013, **446**, 181-188.
3. H. Fan, N. Wang, S. Ji, H. Yan and G. Zhang, Nanodisperse ZIF-8/PDMS hybrid membranes for biobutanol permselective pervaporation, *Journal of Materials Chemistry A*, 2014, **2**, 20947-20957.
4. G. Wu, X. Lu, Y. Li, Z. Jia, X. Cao, B. Wang and P. Zhang, Two-dimensional covalent organic frameworks (COF-LZU1) based mixed matrix membranes for pervaporation, *Separation and Purification Technology*, 2020, **241**, 116406.
5. J. Y. Lee, H. Park, J. S. Lee, S. Yoon and J.-H. Lee, Biphenyl-based covalent triazine framework-incorporated polydimethylsiloxane membranes with high pervaporation performance for n-butanol recovery, *Journal of Membrane Science*, 2020, **598**, 117654.
6. G. Wu, Y. Li, Y. Geng and Z. Jia, In situ preparation of COF-LZU1 in poly(ether-block-amide) membranes for efficient pervaporation of n-butanol/water mixture, *Journal of Membrane Science*, 2019, **581**, 1-8.
7. W. Tang, H. Lou, Y. Li, X. Kong, Y. Wu and X. Gu, Ionic liquid modified graphene oxide-PEBA mixed matrix membrane for pervaporation of butanol aqueous solutions, *Journal of Membrane Science*, 2019, **581**, 93-104.
8. D. W. Mangindaan, G. Min Shi and T.-S. Chung, Pervaporation dehydration of acetone using P84 co-polyimide flat sheet membranes modified by vapor phase crosslinking, *Journal of Membrane Science*, 2014, **458**, 76-85.
9. Y. Luo, S. Tan, H. Wang, F. Wu, X. Liu, L. Li and Z. Zhang, PPMS composite membranes for the concentration of organics from aqueous solutions by pervaporation, *Chemical Engineering Journal*, 2008, **137**, 496-502.

10. Y. Sun, H. Zhao, H. Mao, M. Duan, K. Wang, N. Bao, Z.-P. Zhao and H. Li, Silica hollow spheres-based superhydrophobic PDMS composite membrane for enhanced acetone permselective pervaporation, *Separation and Purification Technology*, 2023, **304**, 122041.
11. L.-H. Xu, S.-H. Li, H. Mao, Y. Li, A.-S. Zhang, S. Wang, W.-M. Liu, J. Lv, T. Wang, W.-W. Cai, L. Sang, W.-W. Xie, C. Pei, Z.-Z. Li, Y.-N. Feng and Z.-P. Zhao, Highly flexible and superhydrophobic MOF nanosheet membrane for ultrafast alcohol-water separation, *Science*, 2022, **378**, 308-313.
12. L. Dai, F. Xu, K. Huang, Y. Xia, Y. Wang, K. Qu, L. Xin, D. Zhang, Z. Xiong, Y. Wu, X. Guo, W. Jin and Z. Xu, Ultrafast water transport in two-dimensional channels enabled by spherical polyelectrolyte brushes with controllable flexibility, *Angewandte Chemie International Edition*, 2021, **60**, 19933-19941.
13. X. Chen, S. Mohammed, G. Yang, T. Qian, Y. Chen, H. Ma, Z. Xie, X. Zhang, G. P. Simon and H. Wang, Selective permeation of water through angstrom-channel graphene membranes for bioethanol concentration, *Advanced Materials*, 2020, **32**, 2002320.
14. J. Kujawa, M. Zięba, W. Zięba, S. Al-Gharabli, W. Kujawski and A. P. Terzyk, Hedgehog-like structure, PVDF- carbon nanohorn hybrid membranes for improved removal of VOCs from water, *Chemical Engineering Journal*, 2022, **438**, 135574.
15. G. Dong, H. Nagasawa, L. Yu, M. Guo, M. Kanezashi, T. Yoshioka and T. Tsuru, Energy-efficient separation of organic liquids using organosilica membranes via a reverse osmosis route, *Journal of Membrane Science*, 2020, **597**, 117758.